

## Ocean's response to Hurricane Frances and its implications for drag coefficient parameterization at high wind speeds

S. E. Zedler,<sup>1,2</sup> P. P. Niiler,<sup>1</sup> D. Stammer,<sup>3</sup> E. Terrill,<sup>4</sup> and J. Morzel<sup>5</sup>

Received 20 November 2008; revised 5 February 2009; accepted 16 February 2009; published 25 April 2009.

[1] The drag coefficient parameterization of wind stress is investigated for tropical storm conditions using model sensitivity studies. The Massachusetts Institute of Technology (MIT) Ocean General Circulation Model was run in a regional setting with realistic stratification and forcing fields representing Hurricane Frances, which in early September 2004 passed east of the Caribbean Leeward Island chain. The model was forced with a NOAA-HWIND wind speed product after converting it to wind stress using four different drag coefficient parameterizations. Respective model results were tested against in situ measurements of temperature profiles and velocity, available from an array of 22 surface drifters and 12 subsurface floats. Changing the drag coefficient parameterization from one that saturated at a value of  $2.3 \times 10^{-3}$  to a constant drag coefficient of  $1.2 \times 10^{-3}$  reduced the standard deviation difference between the simulated minus the measured sea surface temperature change from  $0.8^\circ\text{C}$  to  $0.3^\circ\text{C}$ . Additionally, the standard deviation in the difference between simulated minus measured high pass filtered 15-m current speed reduced from 15 cm/s to 5 cm/s. The maximum difference in sea surface temperature response when two different turbulent mixing parameterizations were implemented was  $0.3^\circ\text{C}$ , i.e., only 11% of the maximum change of sea surface temperature caused by the storm.

**Citation:** Zedler, S. E., P. P. Niiler, D. Stammer, E. Terrill, and J. Morzel (2009), Ocean's response to Hurricane Frances and its implications for drag coefficient parameterization at high wind speeds, *J. Geophys. Res.*, 114, C04016, doi:10.1029/2008JC005205.

### 1. Introduction

[2] It is well established that the drag coefficient increases with wind speed over a range from below 10 m/s up to at least 20 m/s [Wu, 1980; Smith, 1980; Large and Pond, 1981; Yelland et al., 1998]. But the change in the coefficient at higher wind speeds is not well understood because of a paucity of measurements [Powell et al., 2003; Donelan et al., 2004; Black et al., 2007; Jarosz et al., 2007]. At the sea surface, energy that is released from the ocean to a hurricane through evaporation of warm surface water, is dissipated as a shear stress through forcing of a wake of surface and internal waves, and forcing and dissipation have to be in quasibalance to sustain the tropical storm. In a theoretical calculation it was concluded that if the drag coefficient would increase following an extension of the linear relationship in the study by Large and Pond [1981] to wind

speeds higher than 26 m/s, category IV and V storms would require an unrealistic amount of heat input to sustain shear stress and form drag dissipation at the sea surface [Emanuel, 1995]. It follows that the relation between wind stress and wind speed at the level of hurricane strength winds could be very different from that predicted by extrapolating the drag coefficient parameterization for wind speeds below 26 m/s.

[3] Previous in situ and laboratory estimates of the drag coefficient at hurricane strength winds provided evidence for this hypothesis. Using data from GPS dropsondes deployed in 15 hurricanes, Powell et al. [2003] estimated the drag coefficient as a function of wind speed and reported that it would level off for wind speeds exceeding 30 m/s at a value bounded between  $1.3 \times 10^{-3}$  and  $2.3 \times 10^{-3}$ . A similar relationship was established in laboratory experiments [Donelan et al., 2004], in which the drag coefficient, calculated indirectly from a momentum balance for wind speeds higher than 25 m/s, leveled off at  $2.4 \times 10^{-3}$  for wind speeds of 33 m/s, and remained approximately constant as the wind was increased up to 50 m/s. More recently, in situ measurements of flight level velocity fluctuations were made in a hurricane using the Best Air Turbulence probe as part of the Coupled Boundary Layers/Air-Sea Transfer (hereafter referred to as CBLAST) program. The investigation suggests that the drag coefficient saturates for wind speeds exceeding 20 m/s [Black et al., 2007].

[4] All these recent attempts to determine the drag coefficient as function of wind speed, though fraught

<sup>1</sup>Physical Oceanography Research Division, Scripps Institution of Oceanography, La Jolla, California, USA.

<sup>2</sup>Now at Institute of Applied Mathematics and Computational Science, Texas A&M University, College Station, Texas, USA.

<sup>3</sup>Institut fuer Meereskunde, Zentrum fuer Meeres- und Klimaforschung, Universitaet Hamburg, Hamburg, Germany.

<sup>4</sup>Coastal Observing Research and Development Center, Scripps Institution of Oceanography, La Jolla, California, USA.

<sup>5</sup>Rosetta Consulting, Boulder, Colorado, USA.

somewhat with data interpretation problems in the air above water, suggest that it asymptotes to a constant level at high wind speeds. Estimates differ, however, in the critical wind speed and the amplitude at which the drag coefficient levels off (in principle this could be a function of surface wave spectrum). The variability among these results can be attributed in part to differences in the experimental approaches taken. For example, as acknowledged by *Powell et al.* [2003], drag coefficient estimates derived from GPS dropsonde velocity profile measurements are thought to be biased low because of the minimizing effect of inward radial advection of the sensor on the vertical shear in the measured wind speed. In a laboratory tank setup such as adopted by *Donelan et al.* [2004], waves are likely in equilibrium with the wind, which may not be the case in the real ocean. Direct flight level turbulence measurements such as collected by *Black et al.* [2007], require the assumption that they are constant over the height of the boundary layer and can be divided by radar derived wind speed estimates at 10 m to retrieve a reliable estimate of the drag coefficient. Although estimating the amount of energy dissipated through shear stress at the sea surface is an important parameter for understanding and predicting the intensity of a tropical storm [*Black et al.*, 2007], the question of what the drag coefficient would be at high wind speeds is still open.

[5] The use of well-supported models offers an alternative approach to estimating the drag coefficient. The wind stress forcing in an ocean model may be adjusted so as to minimize the difference between in situ measurements of upper ocean temperature and velocities taken underneath a hurricane passage and the corresponding model simulations under realistic conditions [*Jarosz et al.*, 2007]. Assuming that the wind vector at 10 m height above the surface,  $U_{10}$ , is known and that the model is perfect, then an estimate can be made of the drag coefficient relationship with wind speed. Ideally such an effort should be performed in the context of ocean state estimation where the wind stress (and if the 10 m velocity field is given, actually the drag coefficient) is being adjusted along with other variables as control parameters so as to best simulate ocean observations [*Stammer et al.*, 2004; *Stammer*, 2005]. An alternative, and logistically simpler, approach is to perform forward (process oriented) model sensitivity studies by comparing the model's response to changes in the drag coefficient and then to the wind stress field against observations.

[6] As a first step in the latter direction, *Sanford et al.* [2007] ran a high-resolution model (10 km in the horizontal, 5 m in the upper 100 m of domain) in forward mode and compared results with upper ocean stratification and velocity profiles measured by three profiling floats underneath Hurricane Frances, as part of the CBLAST experiment. The mixing parameterization used was PWP [*Price et al.*, 1986] and the wind stress used to force the model was computed using two different drag coefficient parameterizations following *Large and Pond* [1981] and *Powell et al.* [2003]. The authors concluded that the ocean response in terms of temperature and vertically integrated velocity transport per unit meter, was consistent with observations for a drag coefficient relationship by *Powell et al.* [2003], and was grossly overestimated when the relationship by *Large and Pond* [1981] was implemented.

[7] In this paper, we expand on the previous effort of *Sanford et al.* [2007], by comparing model simulations, based on the MIT/OGCM, with a larger set of data collected underneath Hurricane Frances during August. Our specific goal is to investigate the sensitivities of the model's response to the wind stress that results from a NOAA-HWIND product available for Hurricane Frances using four different drag coefficient parameterizations (as function of wind speed) and test the respective model simulations against those measured temperature and velocity fields. It should be noted here that the ocean responds to the wind stress, and the ability to conclude that differences in the simulated versus measured fields result from the different drag coefficient parameterization per se relies on our confidence in the wind speed field. The NOAA H\*WINDS are computed using an objective mapping of available wind speed measurements from a variety of platforms. The accuracy of the product depends on the available data, which varies from one snapshot to the next. Although we do not have error bounds on the wind speed field used in this study, we discuss the wind speed field in the appendix. We have included a table that lists the available sensors used for modeling the wind speed field for Hurricane Frances.

[8] The remainder of the paper is organized as follows: In section 2 we summarize the database available as ground truth information underneath Hurricane Frances. Section 3 describes the model setup and the experiments performed. Section 4 summarizes the model's response to strong wind-forcing. The sensitivity of the model results to details of the drag coefficient is discussed in section 5. The sensitivity of the model to other uncertain model parameters, such as mixing parameterization, is discussed in section 6. Conclusions are given in section 7.

## 2. Data Base

[9] The ground truth data for our model sensitivity study were obtained underneath hurricane Frances as part of the CBLAST experiment from an array of 22 drifters fitted with thermistors at the surface, 14 of which were drogued to 15 m depth, and 12 profiling floats. The instruments were deployed on 31 August 2004, from a C-130 aircraft in a region just to the northeast of the Caribbean Leeward Island chain for an area bounded between  $69^{\circ}$ – $72^{\circ}$ W and  $21.5^{\circ}$ – $24^{\circ}$ N [*Black et al.*, 2007]. Seven additional drifters deployed by ship in July 2007 were also in this area.

[10] In this study we use temperature data collected from all floats and a subset of 22 drifters, all of which were located within 200 km on the right side of the storm track, along with velocity estimates based on position data from 12 of the drifters drogued at 15 m (Figure 1). Prior to the storm passage, the temperature field in the upper 200 m, as documented by the floats, was roughly uniform over the sampling area. From the surface drifter the SST was subsampled at approximately 50 km resolution. The floats were split into two groups centered at  $70^{\circ}$ W and  $71^{\circ}$ W, respectively. The surface position of the floats and drifters was tracked by the ARGOS satellite, which has an average position error of 350 m. The 12 Minimet drifters fitted with GPS receivers, though only operational during part of the

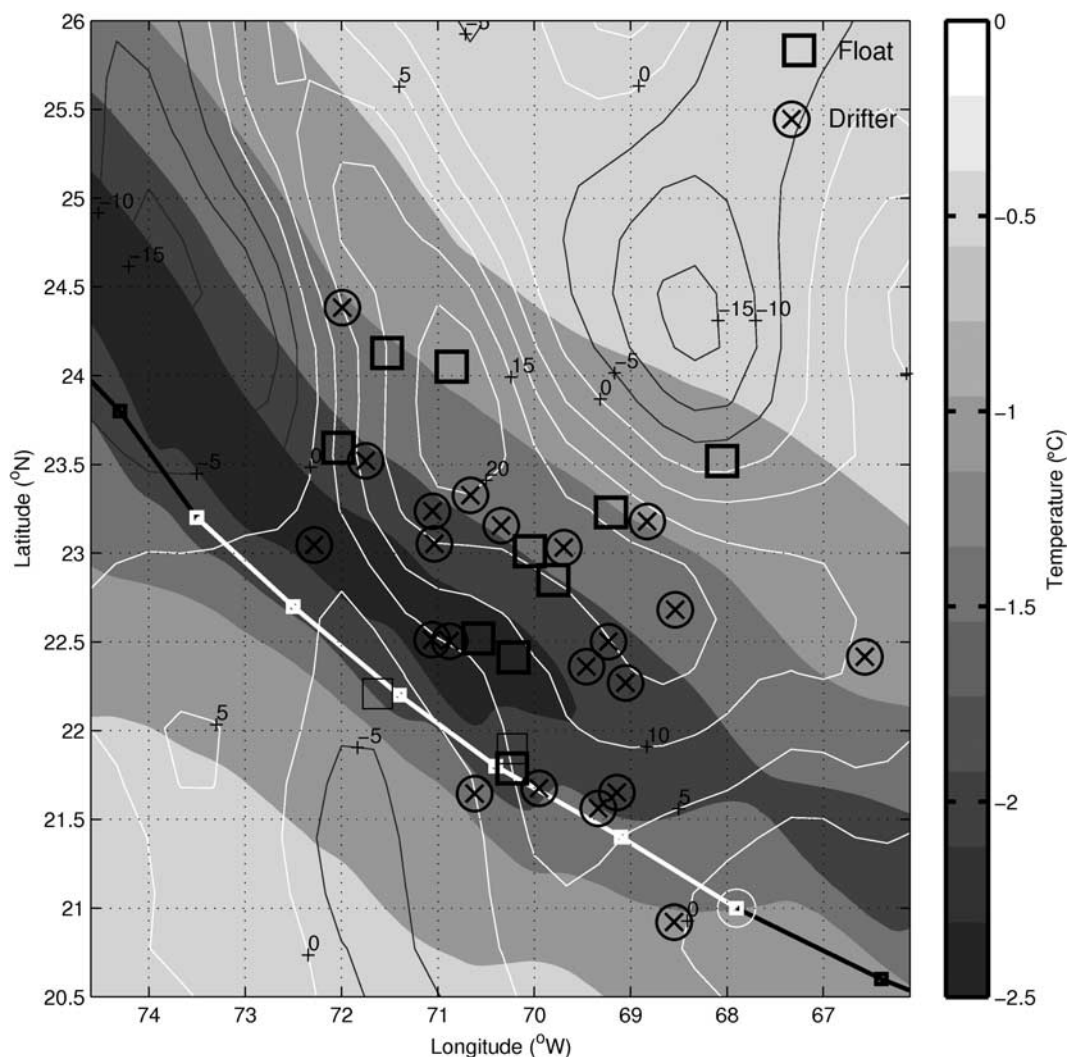


**Figure 1.** Plan view of simulated sea surface temperature wake as forced by NOAA HWINDS and using CBLAST drag coefficient parameterization, with average position of floats and drifters over 1 day centered at 1.5 days after the passage of Hurricane Frances. Contour lines represent sea surface height anomaly as provided by the AVISO sea surface height product (<http://www.jason.oceanobs.com>). Positive and negative anomalies are colored white and black, respectively. Note the region of positive anomalies directly to the right of the storm track, suggesting the presence of a warm core feature.

deployment period, had decreased position error to about 100 m.

[11] Drifters and floats closely followed the streamlines of a mesoscale eddy situated around 100 km to the northeast of the storm track after the passage of Frances. This feature had a 20 cm sea surface height anomaly and a velocity anomaly of 20–40 cm/s as is typical for mesoscale eddies at this latitude. Estimates of the storm translation velocity were obtained by taking simple difference derivatives of the central positions of the storm along its path provided by <http://www.prh.noaa.gov/cphc/pages/glossary.php>. Our estimate suggests that the storm was slowing down as it approached the instrument array from the east from a translation speed of 7 m/s to 5.5 m/s. The storm translation speed is an important parameter for determining the sea surface temperature response because slower storms pro-

duce enhanced entrainment at the base of the mixed layer [Greatbatch, 1984].

### 3. Model Setup and Experiments

#### 3.1. Model Setup

[12] For our study, the MIT OGCM [Adcroft, 1995] was implemented with a  $1/12^\circ$  horizontal resolution and 20 vertical layers (10 m in the upper 100 m, to 500 m at the bottom) in a spatial domain of extent  $45^\circ$  in longitude and  $30^\circ$  in latitude, east of the Caribbean Leeward Island chain ( $43^\circ$ – $88^\circ$ W,  $7^\circ$ – $37^\circ$ N). As described in detail by Marshall *et al.* [1997a, 1997b], the MIT OGCM ocean model is based on the Navier Stokes equations for an inviscid, Boussinesq, hydrostatic, and incompressible fluid. Shear instability type vertical mixing is parameterized using the KPP turbulence closure model [Large *et al.*, 1994]. The model was run with a free surface on a spherical grid. Values for the background

vertical viscosity and diffusivity were chosen to be  $1 \times 10^{-4} \text{ m}^2/\text{s}$  and  $1 \times 10^{-6} \text{ m}^2/\text{s}$ , respectively. Horizontally, coefficients for harmonic forms of viscosity and diffusivity had an amplitude of  $5 \times 10^9 \text{ m}^4/\text{s}$ . The Caribbean Leeward Island chain was represented by a straight vertical wall in the southeast corner of the domain extending across a straight line between ( $88^\circ\text{W}$ ,  $24^\circ\text{N}$ ) and ( $58^\circ\text{W}$ ,  $15^\circ\text{N}$ ). A no-slip boundary condition was imposed along these solid sidewalls. All other boundary conditions were doubly periodic, but the domain was chosen to be large enough to minimize reflection of waves at lateral boundaries over a period of 5 days as the hurricane passed through this domain. For the region not covered by land, the bottom topography was flat and at a depth of 2000 m.

[13] For all basic experiments the horizontally uniform, initial temperature and salinity fields were based on hydrographic measurements collected from the profiling floats (0–200 m) and from CTD casts taken during August, 2002 (200 m ocean float). The 9 CTD casts were conducted as part of the World Ocean Circulation Experiment (<http://woce.nodc.noaa.gov/wdiu/>). The float profiles collected on 30 August 2004, and CTD profiles collected on an east-west cruise track during 12–20 August 2002, taken respectively, were averaged into mean profiles for the upper (0–200 m; Figure 2), and for the lower (600–2000 m), regions of the ocean. The temperature and salinity profiles were linearly interpolated in the intermediate depth region (200–600 m). The composite profile was then linearly interpolated to the model grid.

### 3.2. Experiments

[14] All experiments performed in this study are summarized in Table 1 and differ only in their wind stress and heat flux forcing fields, and storm track, as described in Appendix A. The wind speed field was based on the NOAA HWIND product for Hurricane Frances, available at six hourly intervals (<http://www.aoml.noaa.gov/hrd/>). The storm position and wind speed fields were interpolated linearly in time at the 240 second model time step. For each experiment, one of four drag coefficient parameterizations (Figure 3), was used in the calculation of wind stress (see Figures 3b and 3c). Three of these functions were based on relationships derived from field or laboratory measurements [Powell et al., 2003; Donelan et al., 2004; Black et al., 2007] and are presented in Table 5 for *CBLAST* and *Powell*, and equation (A2) for *Donelan*. Note that all drag coefficient values for wind speeds below 20 m/s are close to or exactly match those from the *Large and Pond* [1981] relationship. The fourth drag coefficient was kept at a constant value of  $1.2 \times 10^{-3}$  for all wind speeds. The results from the experiments *Constant*, *Donelan*, *Powell*, and *CBLAST* are then compared with observed upper ocean temperature and current responses to Hurricane Frances to determine which simulation agrees best with the Hurricane Frances observations.

[15] For temperature comparisons, our measure of best fit is the smallest standard deviation (STD) difference in the ensemble of time-averaged in situ poststorm sea surface (drifters) or upper ocean (floats) temperature anomaly (relative to the initial value). The temporal average was taken over an interval of a day, centered 1/2 day after the storm passage. This was determined individually for each

time series. For the floats, the temperature change was additionally averaged over the upper 20 m. Since the prestorm and poststorm water column were well mixed to below 20 m, the depth averaged temperature change was within  $0.1^\circ\text{C}$  of the sea surface temperature.

[16] Velocity estimates are also compared from simulated and actual drifters. For the actual drifters, we calculated velocity estimates using simple differencing of position fixes and then band-passed these over the frequency range of  $0.5f_{22N}$ – $1.5f_{22N}$  to remove low-frequency fluctuations likely associated with mesoscale eddies. Simulated drifter time series of velocity, as output by the model, were band-passed filtered over the same frequency interval. The simulated drifter time series were extracted from the model domain by linear interpolation at the actual drifter and float locations.

[17] Two extra experiments were performed subsequently in a somewhat simplified setting, to test the model sensitivity to details of the turbulent mixing parameterization. Both experiments were configured in a 35 vertical level (ranging in height between 5 m in the upper 100 m to 500 m), 2000 m flat-bottomed f-plane domain at  $22^\circ\text{N}$  with dimensions 2000 km in the east-west direction by 3000 km in the north-south direction and 10 km horizontal resolution. The first of those experiments, *PWP*, was run using the three-dimensional PWP hurricane model that is described by Price et al. [1994]. This is a version of the same model used for the calculation made by Sanford et al. [2007] that implements the PWP algorithm for turbulent mixing [Price et al., 1986] and a radiation boundary condition at the edges. The second experiment, *MIT*, used a regional version of the MIT OGCM that implements the KPP turbulent mixing parameterization with doubly periodic boundary conditions. For both experiments the horizontally uniform, initial temperature and salinity fields were interpolated linearly from vertical profiles based on initial stratification measured prior to the passage of Frances (see <http://www.whoi.edu/sbl/liteSite.do?litesiteid=8232&articleId=12187>).

[18] The radial profiles of wind speed and of inflow angle of the wind vector toward the center of the storm (in a frame of reference stationary relative to the storm) are based on the NOAA-HWINDS product for Frances as it approached the CBLAST instrument array from the east in early September (see <http://www.whoi.edu/sbl/liteSite.do?litesiteid=8232&articleId=12187>). The storm is translated directly to the north in the center of the grid at a constant speed of 5.5 m/s and in both experiments the drag coefficient parameterization used to convert wind speed components to stress is based on the results by Powell et al. [2003].

[19] Differences between experiments *MIT* and *PWP* were evaluated by comparing an east-west cross section of the sea surface temperature anomaly relative to the initial condition that was extracted from each model and averaged over 1.33 days (i.e., the inertial period at  $22^\circ\text{N}$ ).

## 4. Temperature Response

[20] The 12 floats used for a comparison of model simulations with observations were grouped according to their approximate distance from the storm track, as presented in Table 2. Because the measured and simulated

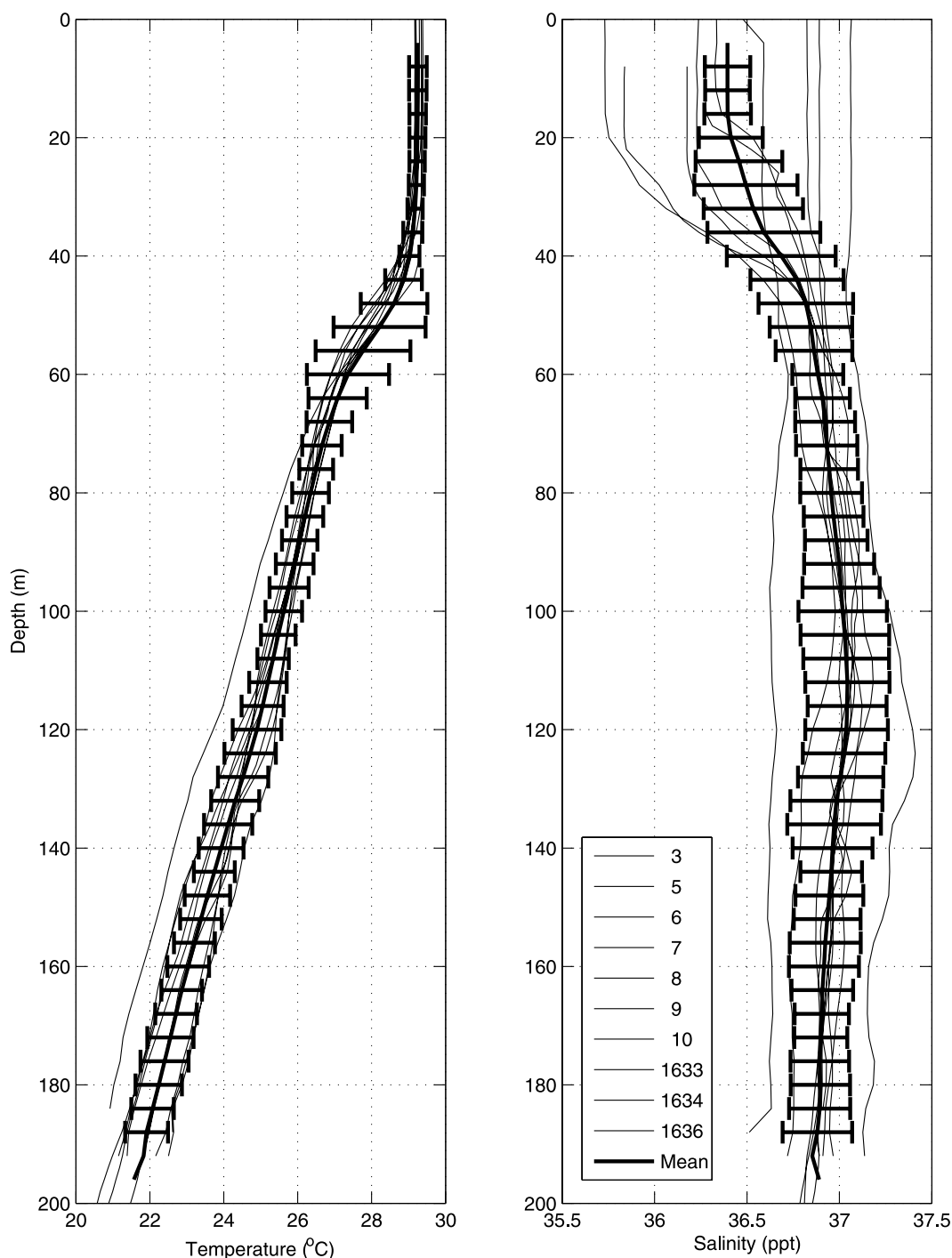


**Figure 2.** (left) Average and standard deviation of temperature profile for each of 10 profiling floats from 30 August 2004; black thick line is ensemble average of all, used for the composite profile. (right) Same, for salinity.

temperature response within each group was similar, we show time series only from floats 2, 7, 3, 5, and 9 as typical examples of the response at distances of 0, 50, 100, 150, and 200 km away from the storm track, respectively.

[21] 1. Floats 2, 8, and 36 (group 1) were situated directly beneath the center of the storm track, and exhibited the largest temperature change at 150 m depth during the storm passage, as well as the strongest vertical fluctuations of (thermocline) isotherms at the near-inertial period (Figure 4a). Mixed

layer temperature decreased by a maximum of  $2.3^{\circ}\text{C}$  and isotherms in the thermocline fluctuated vertically by as much as 60 m.

[22] 2. Floats 7, 4, and 33 were located about 50 km to the right of the storm track underneath the band of maximum winds, and exhibited a large change in the mixed layer temperature and moderate vertical fluctuations of the isotherms (Figure 4b).

**Table 1.** Experiments Performed in This Study<sup>a</sup>

Name	$C_d$ Type	$U_s$	Mixing Type	Storm Heading
Donelan	<i>Donelan et al.</i> [2004]	variable	KPP	NOAA best track
Powell	<i>Powell et al.</i> [2003]	variable	KPP	NOAA best track
CBLAST	<i>Donelan et al.</i> [2004]	variable	KPP	NOAA best track
Constant	$1.2 \times 10^{-3}$	KPP	variable	NOAA best track
MIT	<i>Powell et al.</i> [2003]	5.5 m/s	KPP	directly north
PWP	<i>Powell et al.</i> [2003]	5.5 m/s	PWP	directly north

<sup>a</sup>The simulation names, drag coefficient parameterization with wind speed, storm translational speed, turbulent mixing parameterization, and storm track have column labels Name,  $C_d$  Type,  $U_s$ , Mixing Type, and Storm Heading, respectively. NOAA best track refers to the best track for Hurricane Frances, as reported on the National Hurricane Center website (<http://www.nhc.noaa.gov/2004frances.shtml>; interpolated linearly in time at 240-s intervals), and NOAA best track refers to the path from the time series of wind speed provided by NOAA HWINDS (described in Appendix A).

[23] 3. Floats 3, 10, and 34 were positioned 100 km from the storm track, and exhibited small changes in the mixed layer temperature and small vertical excursions of the isotherms (Figure 4c).

[24] 4. Floats 5 and 9 were further away than 150 km from the storm track, and showed the smallest changes during the storm passage (Figure 4d).

[25] 5. Float 6 was about 200 km away from the storm track, but was deployed furthest to the west. The somewhat enhanced response for sea surface temperature observed at this float may be due to the observation that the storm passed over this instrument more slowly than over the other floats (Figure 4e).

[26] Simulated float time series are constructed by interpolating the model data spatially and temporally (using a linear weighted average in time) at the exact ARGOS telemetered position of the actual floats (shown in the wind stress forcing case implemented with a constant drag coefficient in the left hand column of Figure 4). In general, there is good agreement between simulated and actual temperature profile time series at the float locations. Specifically, the magnitudes of the mixed layer cooling during the storm passage and of the isotherm fluctuations are similar during the first couple of days subsequent to the storm passage. During later times, vertical excursions of the seasonal thermocline are larger in the simulated drifter temperature fields than in the observations. The phases of the vertical fluctuations of the isotherms in the thermocline show favorable agreement in the simulated and measured float time series. The isotherm fluctuations in the thermocline can be interpreted to result from convergence and divergence of the near-inertial currents generated in the mixed layer (i.e., inertial pumping [Price, 1983]). In the model, the temperature change in the mixed layer is a result of lateral advection, vertical mixing, and heat transfer to the atmosphere.

[27] There are also higher frequency fluctuations visible in the measured temperature profiles, which are absent in the simulated fields. Two likely sources for this difference are aliased internal waves and the presence of mesoscale eddy signals in the observations, neither of which were simulated in the model. In addition, the sampling methods are different: (1) the model output has been averaged over 1-hour intervals from output provided every 240 seconds, whereas the field data profiles are sampled continuously with depth, and taken at 2 or 4 hour intervals and (2) the floats are advected horizontally by the mesoscale back-

ground flow during their vertical profile descent (i.e., travel at an angle to the vertical), whereas the simulated profiles are vertical. Concerning point (1), the floats take approximately 30 minutes (0.1 m/s vertical velocity) to complete a vertical profile, and are not capturing signal at frequencies higher than 1 cycle/hour. This sampling frequency is well below the local maximum buoyancy frequency for internal waves of 11 cycles/hour, which serves as the upper threshold frequency for random trains of internal waves in this stratification environment. Concerning point (2), noise could also be introduced into the float measurement from sloping isopycnal surfaces associated with the background mesoscale.

[28] The depth profiles of the temperature anomaly relative to the initial stratification for floats 7, 4, and 33 are shown in Figure 5. The simulated temperature changes are remarkably similar to those observed, and show cooling above scaled depth  $\zeta = z/65 \text{ m} = -1$  (region A) and below  $\zeta = -2$  with net warming in between (region B). In a one-dimensional system, an estimate of the heat lost at the surface could be made by integrating this temperature anomaly profile vertically over the interval  $-2 \leq \zeta \leq 0$  (roughly, the residual of the sum of areas A and B). However, in the wake of Hurricane Frances, the three-dimensional effects of advection of thermal energy (and momentum) cause the isotherms in the thermocline (below  $\zeta = -1.5$ ) to experience a temporal change in cooling over a longer time period of the inertial cycle than heating [Greatbatch, 1983; Niwa and Hibiya, 1997]. In such a fully three-dimensional circulation system as occurs under hurricane forcing, changes in the vertical profile of temperature are due to both advection and mixing processes.

[29] Drifter data show sea surface temperature decreases up to  $2.7^\circ\text{C}$  on a timescale of several hours, which is much shorter than the approximate residence time of the storm. Note that although we show sea surface temperature time series for the raw data, applying a 1-day smoothing filter does not make a significant difference in the estimate of temperature change from the initial condition. There are examples of actual and simulated drifter anomaly time series that agreed very well with one another (Figure 6). However, there are also some examples where the agreement is poor.

## 5. Near-Inertial Currents

[30] After the storm passage, the drifter array roughly followed the velocity field of the mesoscale flow field (Figure 1), and covered most of the area where the model displayed a response in the storm induced temperature field. Some of the drifters, notably 40, 37, and 39, crossed the region of maximum simulated temperature response as they were advected by the mesoscale eddy field. Cyclonic near-inertial oscillations are evident in several of the drifter tracks (e.g., drifters 30 and 35). If the velocity spatial-temporal field were due to motions entirely at the inertial period, the speed would be constant in time around an inertial circle. Following drifter paths, the speed is not constant for model or field data, as seen in Figure 7. In general, the model overestimates the observed near-inertial current speeds. The near-inertial component of current speed generated in a hurricane wake is a function of both

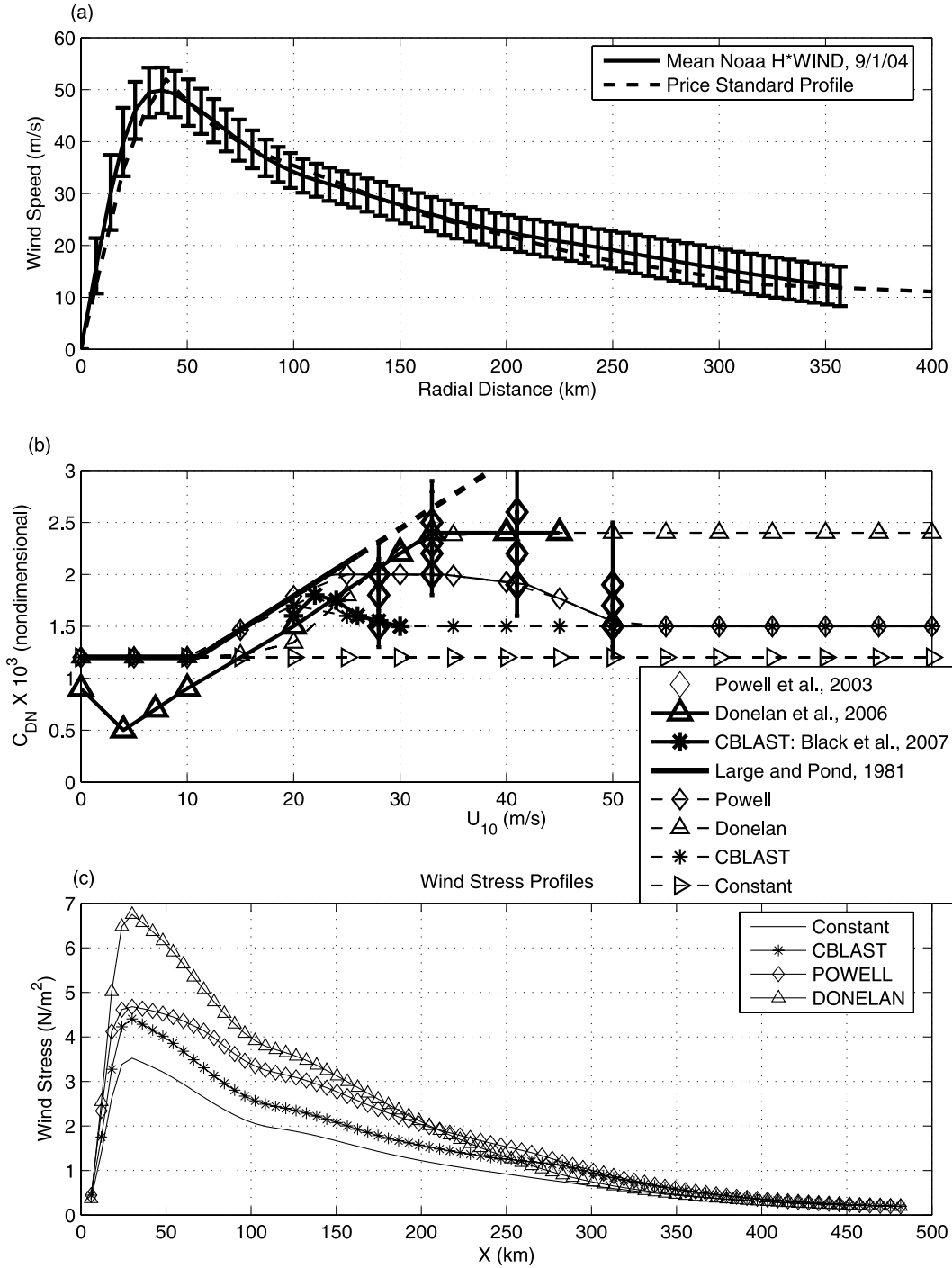


**Figure 3.** (a) Radial wind speed profiles used to generate wind stress for various experiments, as used for intercomparison with the study by [Sanford et al. 2007], a radial average of the wind speed from the NOAA HWIND product (and standard deviation), and from the wind speed product based on drifter measurements. (b) Drag coefficient relationships as a function of wind speed as used in generation of wind stress forcing fields for the four simulations considered in this paper, along with their measurement-based analogs (when applicable) from the studies by Donelan et al. [2004], Powell et al. [2003], and Black et al. [2007]. An extension of the parameterization from the study by Large and Pond [1981] to wind speeds above 25 m/s is shown for reference. (c) Radial wind stress profile on right-hand side of Hurricane Frances from HWINDS on 1 September 2004 at 1:30 GMT, for the four drag coefficient parameterizations.

**Table 2.** Float Number and Approximate Distance From Storm Track 1.5 Days After Storm Passage Through Region

Group	Float ID	Approximate Distance From Storm Track (km)
1	2, 8, 36	0
2	4, 7, 33	50
3	3, 10, 34	100
4	5, 6	150
5	9	200

time (e.g., for Hurricane Felix, mooring measurements of current speed at 45 m had e-folding times of several days [Zedler *et al.*, 2002]) and space. These factors influence temporal fluctuations in filtered current speed amplitudes (e.g., for drifters 30, 31, and 32). With the exception of drifter 31, near inertial simulated and observed drifter speeds decreased significantly between days 8 and 10. This is due to the expected decay of the near inertial wave train in the mixed layer [Price, 1983]. In general, the decay of near-inertial currents was larger in the actual than in the simulated currents.

[31] There are time series that show an excellent agreement between the simulated and observed near-inertial speed, e.g., for drifter 33, and there are time series that agree less favorably, e.g., for drifter 40. However, the least favorable agreement between simulated and measured drifter speeds is arguably for drifters 28 and 38, both of which were located on the left hand side of the track, where the inertial response should be smaller, and where we did not accurately represent the topography of the Caribbean Leeward Island chain.

## 6. Model Sensitivity to Drag Coefficient

### 6.1. Sea Surface Temperature

[32] The standard deviation about the observed storm induced sea surface temperature change ranges from 0.8°C for Donelan-type  $C_d$  forcing to 0.3°C when a constant drag coefficient is used (Figure 8). The sea surface temperature is systematically overestimated for simulations forced with Donelan and Powell models, and the simulated and observed temperature fields agree more favorably in the experiments *CBLAST* and *CONSTANT*. These results call for a drag coefficient that saturates at high wind speeds, as opposed to one that increases with wind speed for hurricane force winds [Large and Pond, 1981], in agreement with Sanford *et al.* [2007]. Furthermore, within the uncertainty of determining the storm induced sea surface temperature change, our results suggest that the drag coefficient either asymptotes to a value below that suggested in the existing observations, or decreases with wind speed [Zhang *et al.*, 2006], in agreement with the estimates by Powell *et al.* [2003] and Jarosz *et al.* [2007], and with the theory supporting that sea spray can play a role in reduction of drag coefficients for hurricane force winds [Bye and Jenkins, 2006; Kudryavtsev, 2006].

### 6.2. Near-Inertial Currents

[33] The relationship between observed and modeled 15 m depth velocity magnitude is nearly linear, with a standard deviation about the data for the Donelan-type  $C_d$  of 12 cm/s, and for the constant  $C_d$  simulation of 5 cm/s, respectively

(Figure 9). When considered in conjunction with the results for the simulated temperature field, this argues for a drag coefficient that saturates at high wind speeds at a value lower than suggested by existing observations, i.e., the availability of additional data enabled us to narrow the drag coefficient to a smaller range of saturation values than was achieved by Sanford *et al.* [2007]. For the experiment with Donelan-type  $C_d$ , the temperature change induced by the storm, as well as the amplitude of the near inertial currents left behind, are both overestimated by a factor of two larger than in the simulation where a constant drag coefficient was implemented. Unfortunately, accurate comparisons of the maximum velocity generated during the residence time of the storm could not be made. During this period, drifter velocities are not reliable because the slip of the drogues in hurricane strength winds has not been measured.

## 7. Model Sensitivity to Mixing Parameterization, Initial Conditions, and Surface Fluxes

[34] Before addressing model sensitivity, we discuss the context within our results should be interpreted. At the outset, the problem of parameterizing the drag coefficient is subject to considerable error. The bulk equation for wind stress magnitude itself

$$\tau = \rho \overline{u'w'} = \rho c_d (U_{10} - U_0)^2 \quad (1)$$

where  $(u', w')$  are the fluctuating horizontal and vertical velocity magnitudes,  $\rho$  is the density of air,  $C_d$  is the drag coefficient,  $U_{10}$  is the horizontal wind speed at 10 m above the surface,  $U_0$  is the horizontal wind speed at the surface, and the overbar implies an average quantity, already introduces many questions. If high frequency velocity data collected from the boundary layer are available, both the length and dimension (i.e., space or time) of the average (indicated by the overbar) must be chosen, and the way these details are handled can result in different calculated stresses. Further errors are introduced when the equation is inverted to calculate  $C_d$ , because the bulk formula for wind stress magnitude is a parameterization. Additionally, the stated formulation (equation (1)) does not take the angle between the wind speed at the surface and the wind speed at 10 m into account, which can be large in a hurricane, but is typically ignored [Powell *et al.*, 2003; Donelan *et al.*, 2004; Black *et al.*, 2007; Sanford *et al.*, 2007; Jarosz *et al.*, 2007]. Observational and modeling studies suggest that the drag coefficient can be quite different when the waves propagate at an angle to the wind [Bourassa *et al.*, 1999; Grachev *et al.*, 2003; Persson *et al.*, 2005]. In this paper, we have compared simulated and measured ocean responses for sea surface temperature and filtered 15 m near inertial current speeds by forcing a model with wind stress calculated using the best wind speed data available and four different parameterizations of the drag coefficient. The fact that any errors in those parameterizations project onto our results warrants caution in their interpretation. We have shown, that the four forcing scenarios produce significantly different responses for sea surface temperature and 15 m currents relative to a ground truth. Our results are consistent with previous research [Sanford *et al.*, 2007]; because of the error germane to any estimate of the drag coefficient, no

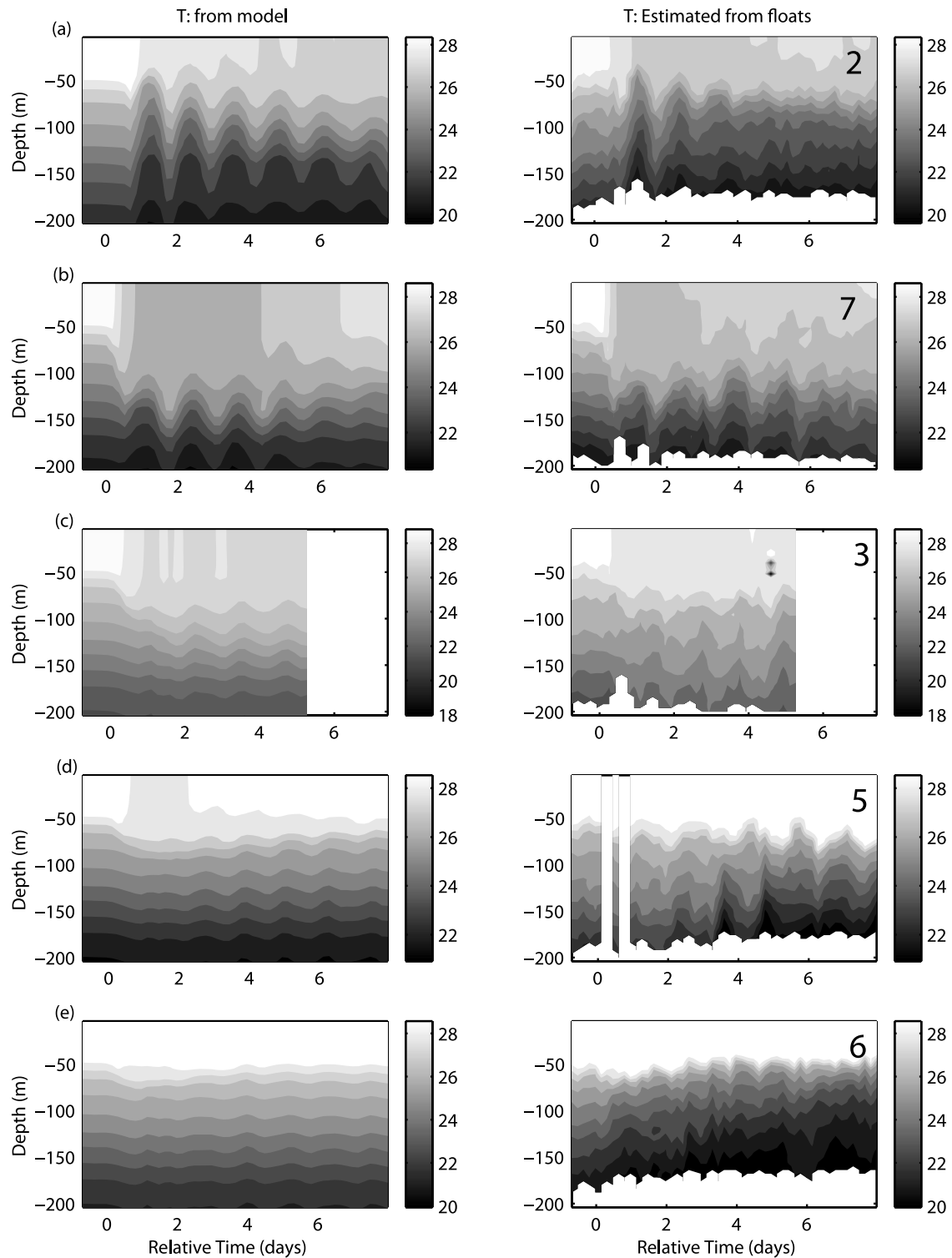


**Figure 4.** (right) Temperature profiles measured by profiling SOLO floats deployed 1–2 days prior to the passage of Hurricane Frances and (left) simulated temperature profiles extracted from the model domain at the equivalent  $(x, y, t)$  positions. See Table 2 for the position relative to the storm track. (a–e) Fields from SOLO floats 2, 7, 3, 5, and 6, respectively. These are spaced at about 50-km intervals at distances to the right of the storm track from 0 to 200 km.

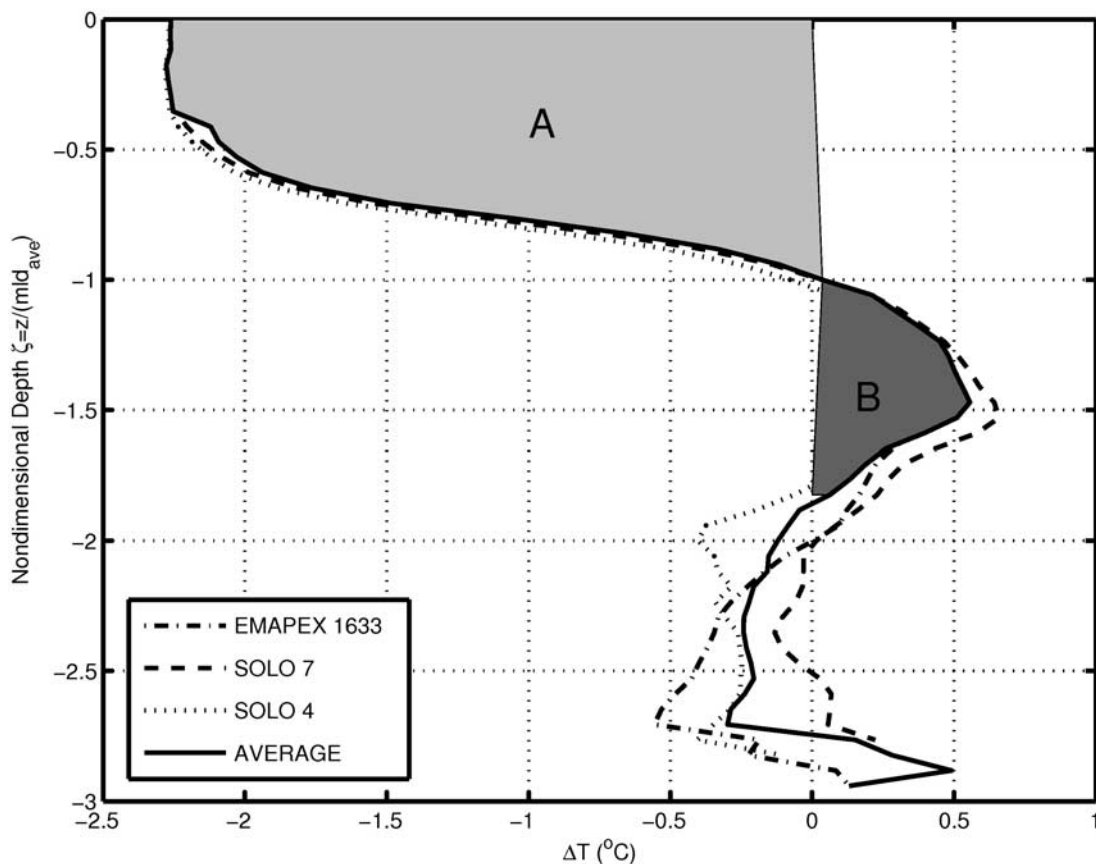


**Figure 5.** Vertical profiles of the temperature anomaly relative to the initial prestorm condition, as measured by floats 4, 7, and 33. After the storm, these floats registered the strongest response for  $\Delta SST$  and were located underneath the band of maximum winds. Before the difference was taken, the poststorm and prestorm profiles were averaged over one inertial period to minimize the effect of upwelling. The depth coordinate has been normalized by the average depth of the mixed layer during the period of mixed layer entrainment (i.e., the storm residence period), so that  $\zeta = 1$  coincides with  $\Delta T = 0$ .

individual study can stand alone, and the best way to make progress is to consider results of multiple approaches collectively, until we can make colocated measurements of flight level wind speed components and turbulence fluctuations at 10 m above the sea surface underneath a hurricane, along with the wind speed at the surface. Our study adds to a growing body of work from different approaches of estimating the drag coefficient at high wind speeds [Powell *et al.*, 2003; Donelan *et al.*, 2004; Black *et al.*, 2007; Sanford *et al.*, 2007; Jarosz *et al.*, 2007]. Our results have utility for coupled models, as they evolve toward higher spatial resolution where hurricanes begin to be resolved. These models calculate wind stress from given wind speed fields and a set parameterization for drag coefficient. Knowing the sensitivity of the modeled response to drag coefficient parameterization at high wind speeds is therefore relevant. Taking the uncertainty in the wind product and drag coefficient parameterization as given, other sources of error in this type of calculation are discussed below.

[35] Our results show that the standard deviation of the simulated surface temperature change minus the measured surface temperature change decreases from  $0.8^{\circ}\text{C}$  to  $0.3^{\circ}\text{C}$  when the drag coefficient is changed from the Donelan *et al.* [2004] formulation to a constant drag coefficient of  $1.2 \times 10^{-3}$  (compare Figure 8). Moreover, we encounter a

systematic overestimation of the observed sea surface temperature change for the Donelan, Powell and CBLAST experiments, and of the observed near-inertial current strength less than 1.5 m/s for all experiments. In performing these sensitivity experiments, we assumed that we have simulated all major features of the storm that contribute to turbulent mixing of the water column. However, the accuracy or realism of model simulations of upper ocean mixing can be affected by a number of factors not considered here, including (1) characterization of the initial model state, (2) detailed knowledge of the forcing fields, and (3) whether parameterizations for turbulent mixing in the model are representative of the processes that cause vertical exchange of momentum and thermal energy on scales smaller than the numerical grid.

[36] Key features of the initial ocean state include horizontal variability in the mixed layer depth, a field of background mesoscale, preexisting wind driven near-inertial currents, and a field of surface waves. In the top 200 m of our region, the initial vertical temperature structure was fairly uniform, whereas the salinity was not (see Figure 2). Specifically, there was a region of low salinity over the top 20 m of water in the region of the warm core eddy feature to the right of the storm, which also appears in the average salinity profile used to initialize our density field (Figure 2).

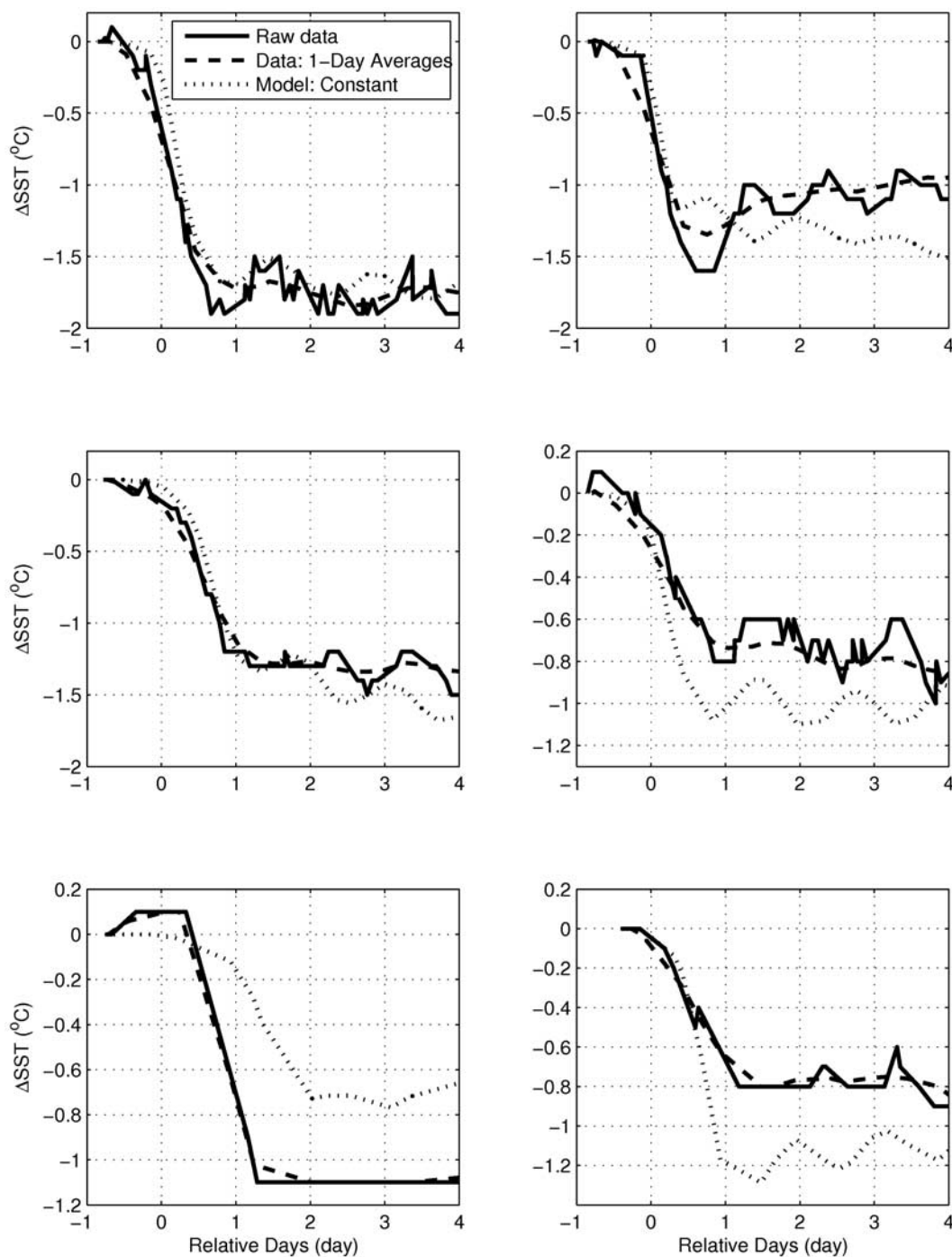


**Figure 6.** Time series of SST anomaly relative to prestorm value for actual and simulated (from experiment Constant) for selected drifters. Relative time is referenced to 1 September 2004, at 11:00 am, when the storm center, as reported by NOAA HWINDS, was positioned at  $-69.9^{\circ}\text{W}$ ,  $21.33^{\circ}\text{N}$ .

The 20 m depth-averaged salinity from the initial profile increases as a function of distance from the storm track. For the group of floats centered at  $70^{\circ}\text{W}$ , and within 100 km of the center of the storm track (including 2, 7, and 3 from Figure 4), the water in the salinity mixed layer is slightly fresher than the initial salinity profile used; for the group of floats initially at distances greater than 100 km from the storm track center, it is slightly more saline (Table 3). Therefore for the floats located less than 100 km from the center of the track, including the spatial variability in

salinity would have the effect of retarding turbulent mixing.

[37] In the KPP module, mixing is parameterized separately for the boundary and interior regions [Large *et al.*, 1994]. In a sensitivity study (not shown), the surface temperatures in our experiments were a maximum of  $0.1^{\circ}\text{C}$  different for simulations performed with the interior mixing turned on and off. Therefore we focus our further discussion of how mixing would be influenced by a shallower initial mixed layer for density in the KPP

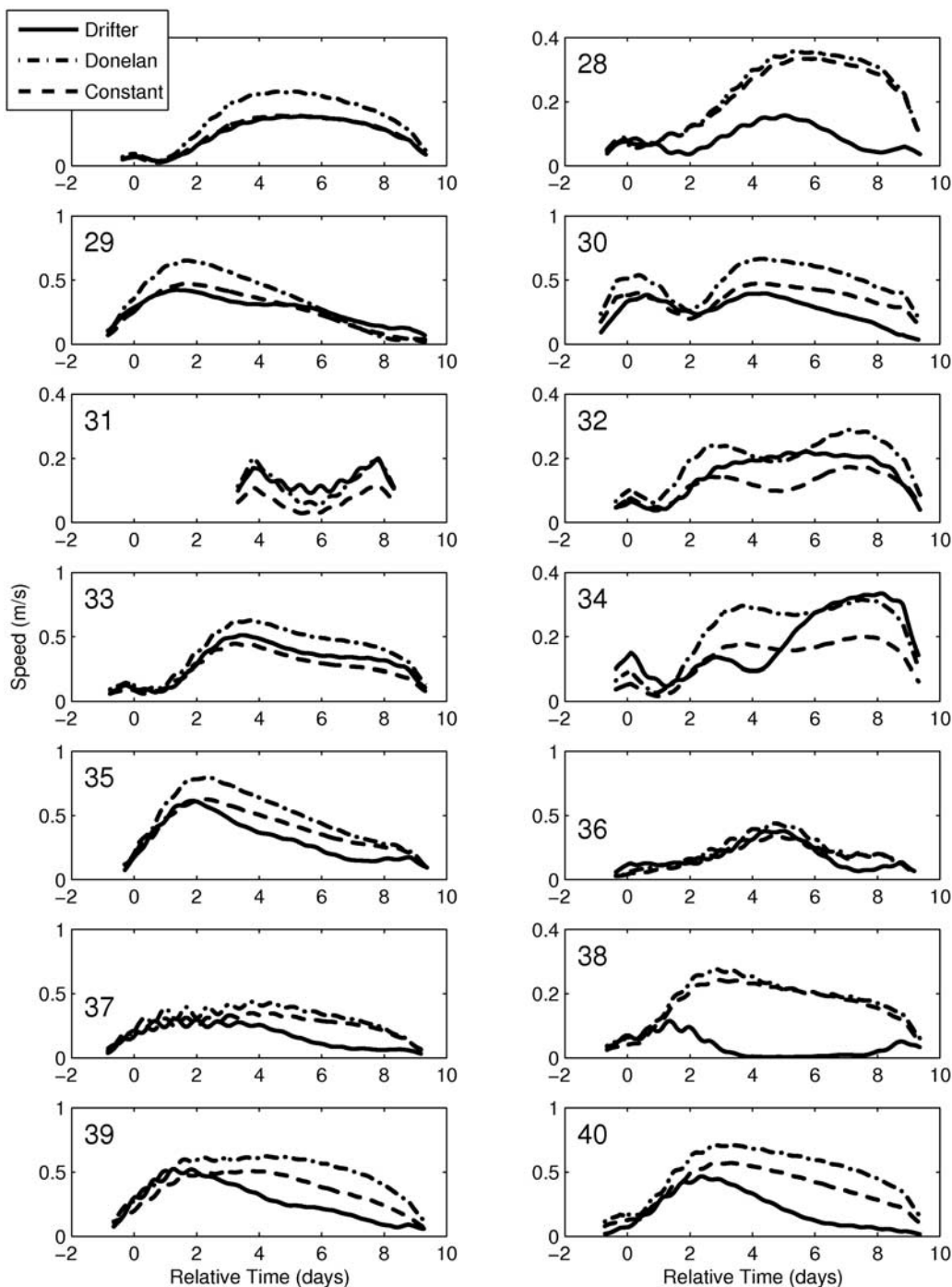


**Figure 7.** Time series of current speed filtered in the near-inertial band from the actual and simulated Minimot drifters. Time series as extracted from the model for simulations forced with Donelan and Constant type wind stress parameterizations. The velocity was calculated using simple differencing of the GPS recorded positions. (a–n) Time series for drifters 27–40, sequentially and respectively. Note that drifters 28 and 38 were deployed on the left-hand side of the storm.

mixing configuration, for which surface layer diffusivities are set as follows

$$K_x = hw_x(\sigma)G(\sigma). \quad (2)$$

In equation (2),  $w_x$  is a scaled vertical velocity depending primarily on surface fluxes of heat and momentum, and  $G(\sigma)$  is a smooth cubic shape function which assumes values of 0 at the surface and at depth  $h$ , and has its maximum at a depth of  $0.3h$ . Variable  $\sigma = d/h$  is the scaled depth  $d$ . Finally,  $h$  itself is the boundary layer

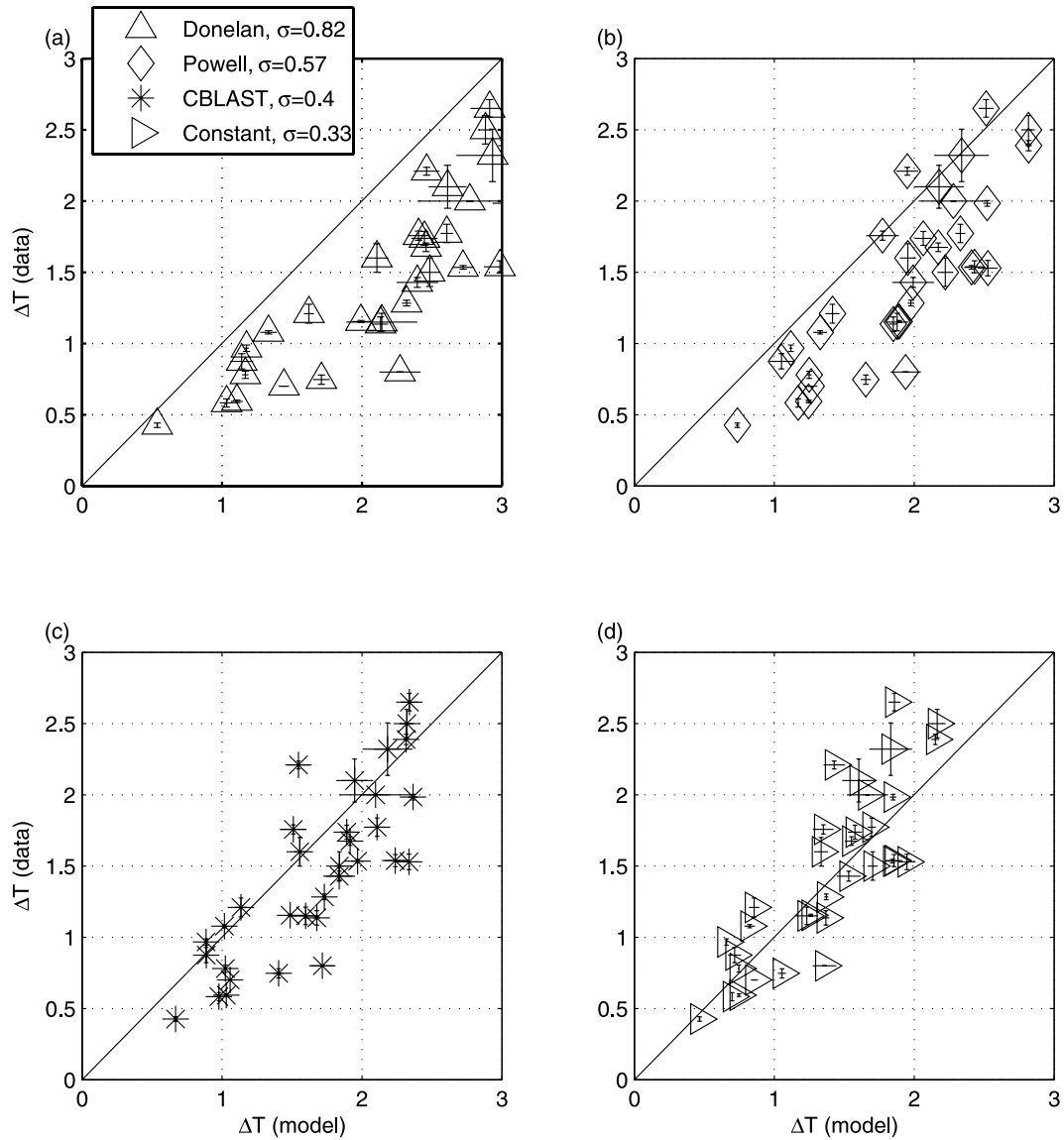


**Figure 8.** Scatterplot of observed (as measured by drifters and floats) 1-day average changes in sea surface temperature (relative to initial condition), plotted against simulated counterpart quantities for four drag coefficient parameterizations based on (a) *Donelan et al.* [2004], (b) *Powell et al.* [2003], (c) *Black et al.* [2007], and (d) Constant drag coefficient (for reference). The error bars are the 90% confidence intervals for the mean.

depth diagnosed as the shallowest depth below which a bulk Richardson number,  $Ri_b$ , satisfies the following inequality

$$Ri_b(d) = \frac{(B_r - B(d))d}{|V_r - V(d)|^2 + V_t^2} \geq 0.3. \quad (3)$$

[38] In equation (2), the buoyancy  $B = \rho(d)g/\rho_0$  (here  $\rho(d)$  is the local density,  $g$  is the acceleration due to gravity, and  $\rho_0$  is a reference density),  $V(d)$  is the current speed at depth  $d$ ,  $V_t$  is a turbulent velocity that is typically large in convectively unstable situations, and the subscript  $r$  refers to the value averaged over a range of near surface reference depths [Large et al., 1994]. For a constant velocity difference of  $|V_r - V(d)| = 0.5$  m/s ( $V_t = 0$ ), and using the range

of initial density stratifications shown in Figure 2, the initial boundary layer depth,  $h$ , calculated from equation (3), had values ranging between 25 m and 50 m. From these equations, it is clear that in the KPP model, the temporal evolution of turbulent mixing would be affected if the spatial variability of the salinity layer in the top 40 m of water were accurately known and simulated. Specifically, the magnitude and location of the maximum diffusivity as initially calculated, would be smaller and shallower, respectively. This is because  $K_x$  is proportional to  $h$ , and because of the way that  $G(\sigma)$  depends on  $h$ . Whether, and by how much, this would affect the net sea surface temperature in the wake would require additional simulations.

[39] The phase of preexisting near-inertial currents has been shown to affect the maximum current generated

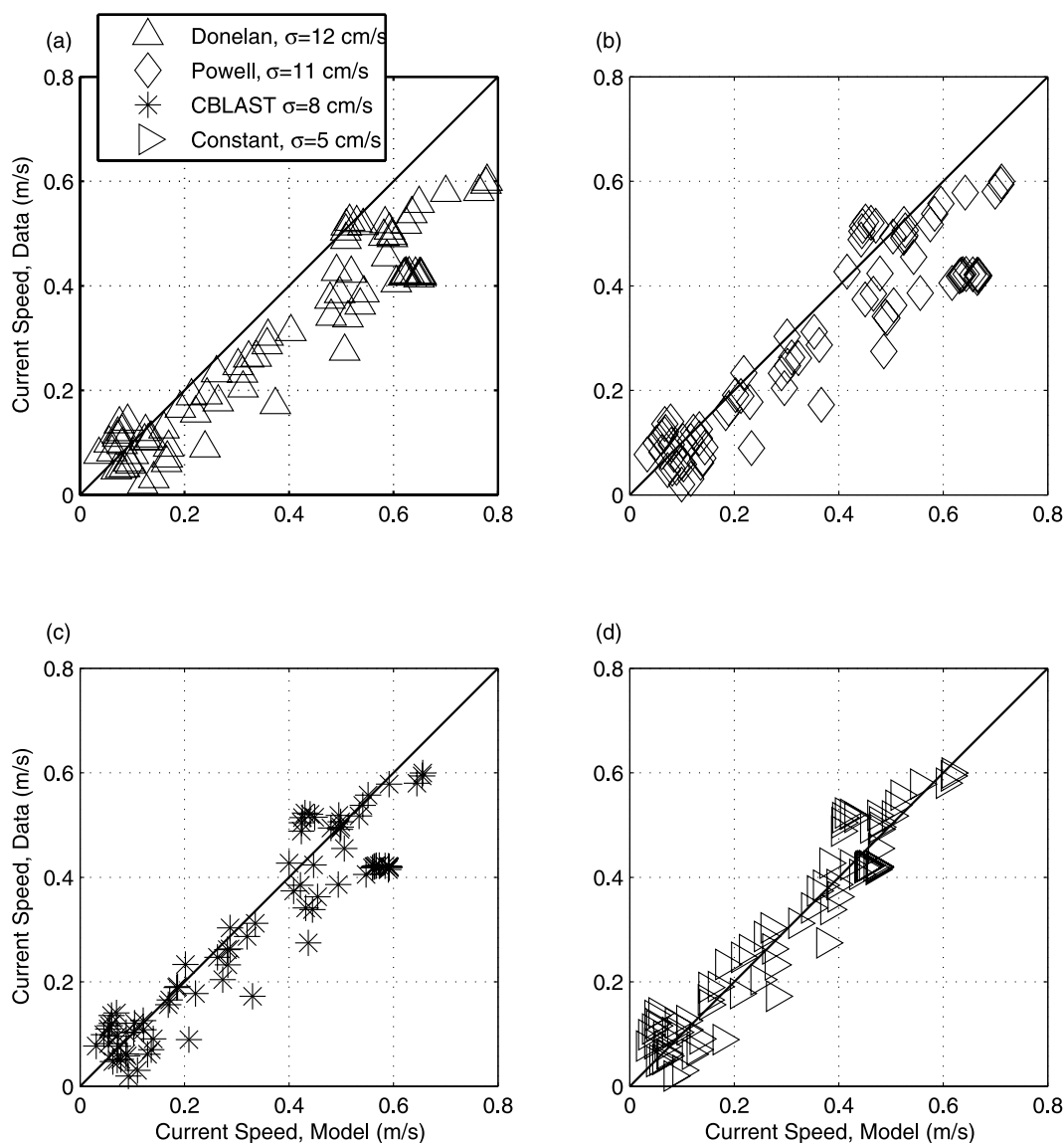


**Figure 9.** Scatterplot of 15-m current fluctuations in the near-inertial band for actual and simulated drifters. Results are shown for simulations forced with four wind stress parameterizations: (a) *Donelan et al.* [2004], (b) *Powell et al.* [2003], (c) *Black et al.* [2007], (d) Constant drag coefficient (for reference).

underneath a hurricane and the magnitude of temperature changes in the near-surface region [Pollard and Millard, 1970; Zedler et al., 2002]. We did not have sufficient current data available to document this effect, although the prestorm current speed measured underneath the band of maximum winds (at the location of float 33) was about 0.3 m/s [Sanford et al., 2007, Figure 3]. If the preexisting currents were out of phase with those generated by the storm, the effect would be a reduction in cooling of the sea surface.

[40] Our study assumes that the structures of wind velocity and heat fluxes are realistic. We did not parameterize precipitation. If the heat fluxes were systematically too high, they could cause overestimation of the mixing due to convective cooling. However, as we found in sensitivity experiments (not shown) the effect of including heat fluxes, relative to excluding them, is only a few tenths of a degree. This is primarily because of the high entrainment flux at the

base of the mixed layer compared to the surface flux [Price, 1981]. Inclusion of fresh water fluxes in a hurricane parameterized following Lonfat et al. [2004] would have a stabilizing effect on the water column (i.e., would retard

**Table 3.** Float Number and Difference in Initial Observed Sea Surface Salinity Relative to Sea Surface Salinity Used to Initialize Model (Horizontally Uniform)<sup>a</sup>

Group	Float ID	Initial $\Delta$ SSS (ppt)
1	8	-0.66
2	7	-0.16
2	33	-0.22
3	3	-0.06
3	34	-0.12
4	5	0.67
4	6	0.50

<sup>a</sup>This is reported for floats deployed near 70°W.

mixing), but in a sensitivity simulation (not shown) the effect on the change in sea surface temperature was less than  $0.1^{\circ}\text{C}$ . Still, if the structure of the wind speed were accurate, uncertainty in the storm translational speed (which sets the residence time) could affect surface temperatures significantly. The NOAA-HWIND wind speed product is provided at six hour intervals, but calculation of the storm speed for Hurricane Frances varies depending on which best track product you use. In a sensitivity experiment for a similar but weaker Category 1 or 2 storm we showed, using the KPP model, that the maximum change in sea surface temperature for a similar storm was  $1\text{--}2^{\circ}\text{C}$  larger when the constant storm translational speed was decreased from  $7.5$  to  $5.5$  m/s, depending on initial stratification and latitude.

[41] Although we cannot determine precisely which processes caused vertical mixing underneath Hurricane Frances, we can assess the sensitivity of the model to turbulent mixing parameterization. For a comparison with our previous results, we therefore used a three-dimensional model implemented with the PWP turbulent mixing model [Price *et al.*, 1994]. In the PWP, density stratification, bulk Richardson number, and gradient Richardson numbers are calculated at each time step for individual profiles and the property tracer is mixed vertically until these quantities are smaller than an upper threshold [Price *et al.*, 1986]. In experiments *MIT* and *PWP*, the simulated sea surface temperature wakes are similar, with the *MIT* exhibiting a maximum of  $0.5^{\circ}\text{C}$  more cooling than the *PWP* on the right hand side of the storm, and approximately  $0.3^{\circ}\text{C}$  more cooling at the location of maximum response, in agreement with the findings of previous turbulent mixing model intercomparison studies (Figure 10; see also [Large and Crawford, 1995; Zedler *et al.*, 2002]). This implies that the best agreement between measured and simulated sea surface temperature for the KPP model should occur at lower wind stress (and hence drag coefficient) values, than for the PWP model. The error introduced by the choice of these two turbulent mixing schemes is comparable to the statistical spread in the simulated, about the observed temperatures, but not necessarily statistically significant. Because turbulence parameterization typically depends on calculation of vertical shear in the horizontal currents (e.g., for the KPP via equation (3) and also parameterizations for mixing in the interior [Large *et al.*, 1994]), there is the possibility that simulated sea surface temperature changes are sensitive to the vertical grid resolution in the surface layer. In sensitivity experiments with vertical grid resolution in the upper 100 m of water of 3 m, 5 m, and 10 m, but otherwise identical in setup to experiment *MIT* (see Table 1), the sea surface temperature change differed by a maximum of  $0.2^{\circ}\text{C}$ . Notably, the change in sea surface temperature was larger everywhere in the domain for the 3 m experiment than for the 5 m experiment, and for the 5 m experiment than for the 10 m experiment. In other words, there was a monotonic increase in the vertical mixing with increased vertical grid resolution, suggesting that if we compared simulated and measured sea surface temperature and 15 m velocity at a higher resolution than 10 m, the result would select for an even smaller drag coefficient at high wind speeds. It must be acknowledged, however, that a difference of  $0.2^{\circ}\text{C}$  is on the order of the error introduced by using different turbulent

mixing parameterizations and of the statistical spread of simulated about the observed temperatures.

[42] The fact that simulated temperatures that most closely matched the measured temperature were 50 km to the right of the storm center, is consistent with rapid change in sea surface temperature during the first approach of the storm followed by a period of much slower changes in sea surface temperature. The reason for the slowdown of the mixed layer temperature decrease is three-fold: (1) Deepening of the mixed layer is coincident with smoothing of the thermocline, with weaker stratification below 60 m for the region underneath Hurricane Frances. (2) The storm residence is not quite as long as the local near inertial period, so that during the passage of the second part of the storm, the currents generated during the passage of the first part of the storm are at an angle to the storm wind (i.e., they are out of phase). For Hurricane Frances, mixing extended to 120 m depth on the right hand side of the storm, well below the region of maximum stratification. (3) As the mixed layer progressively deepens during the storm passage, the stress required to generate the vertical shear in horizontal velocity necessary to cause a unit of overturning increases (this, assuming that the wind stress is absorbed over the entire depth of the mixed layer). However, for a hurricane, the wind stress decreases at distances greater than the radius of maximum winds. Considering these points, the region on the right hand side of the storm, underneath the band of maximum winds, is where we would expect the sea surface temperature change to be least sensitive to application of additional wind-forcing. In the regions where the mixing did not extend to as great a depth, we expect increased sensitivity of the sea surface temperature to errors in the wind stress forcing. This does not explain a systematic bias, but is consistent with our findings.

## 8. Concluding Remarks

[43] An array of profiling floats and drifters documented the temperature and upper ocean current speed before, during, and after the passage of Hurricane Frances through the deployment region. The 10 m wind speed field of Hurricane Frances was parameterized from a combination of in situ measurements (e.g., sea level pressure, direct measurements of wind speed from a C-130 aircraft). This provided the opportunity to compare measured current and temperature fields with simulations forced with four different drag coefficient parameterizations at high wind speeds. We note that our ability to compare our modeling results with observations to choose between drag coefficient parameterizations relies on the accuracy of the wind product. Error bars were not available for NOAA H\*WINDS in 2004, but we have tabulated the available data for Frances and discuss the wind field in the appendix. Our forcing of the MIT OGCM using a variety of wind stress patterns showed the closest agreement between the simulated and measured fields with a drag coefficient parameterization that saturates or decreases at high wind speeds. We therefore agree with the suggestions of Powell *et al.* [2003], Donelan *et al.* [2004], Black *et al.* [2007], and Zhang *et al.* [2006], that linear extrapolation of Large and Pond [1981] to wind speeds greater than 26 m/s is not justified. Large and Pond [1981] to wind speeds higher than 25 m/s). Simulations using the

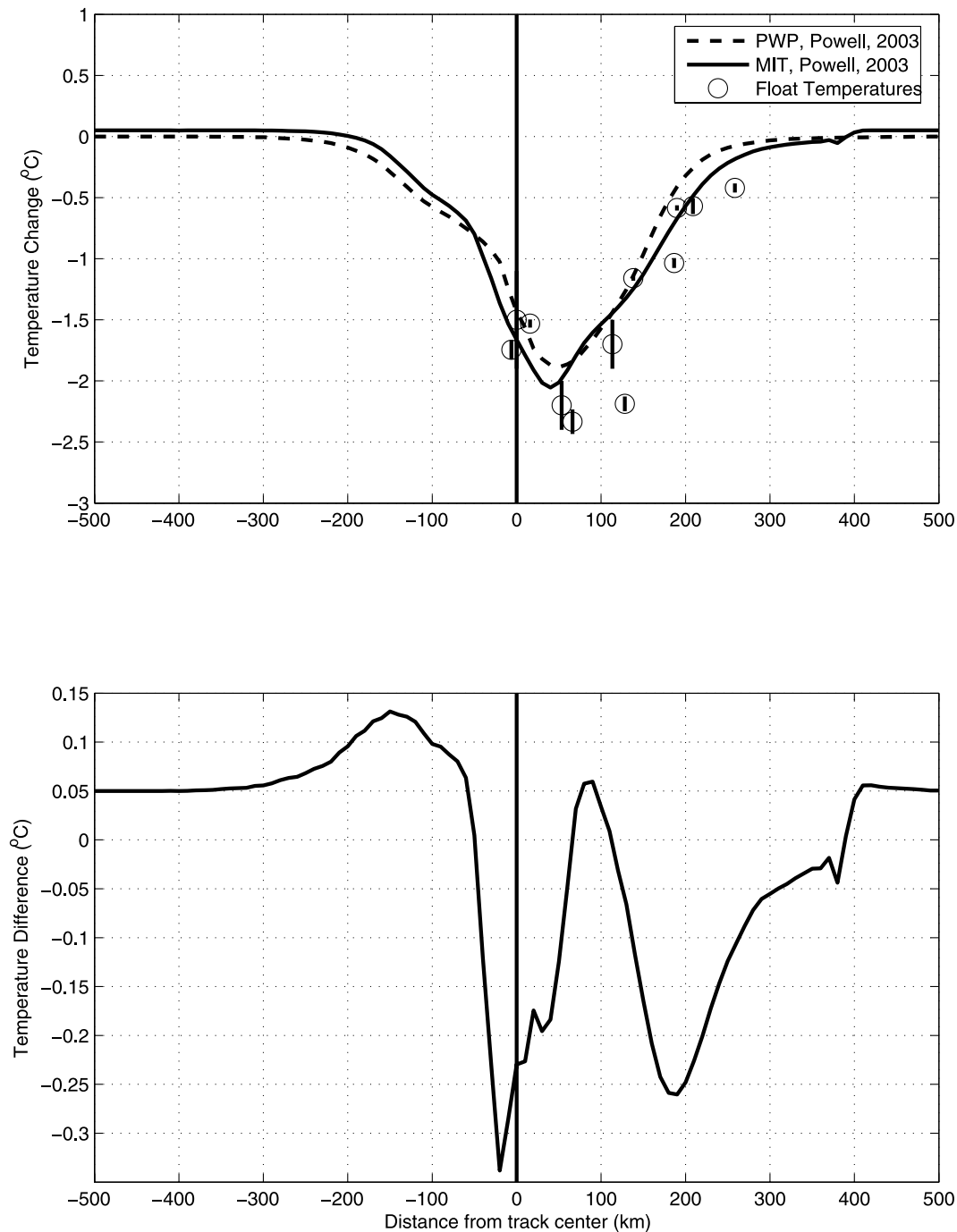


**Figure 10.** (top) Cross-section of change in sea surface temperature averaged over one inertial period for experiment *KPP*, using the MITOGCM implemented with the *KPP* turbulent mixing parameterization [Large *et al.*, 1994] and the *Price et al.* [1994] model implemented with the *PWP* algorithm for turbulent mixing [Price *et al.*, 1986]. The storm was translating on an *f* plane directly north, and the cross-section of temperature is averaged over an inertial period. Temperature changes from the profiling floats, grouped as a function of distance from the storm track, are overlaid. (bottom) Cross-track sea surface temperature difference curve between the two simulations.

MITOGCM model implemented with the *KPP* turbulent mixing scheme generated a very similar temperature response to the three-dimensional model by *Price et al.* [1994] implemented with the *PWP* turbulent mixing parameterization that were initialized and forced with identical conditions. This suggests that the above result is not critically

dependent on the specific choice of the near-surface mixing scheme.

[44] The results are encouraging, but warrant further investigation. As an example, we have identified the horizontal variability of salinity and uncertainty in the storm translational speed as likely candidates for the largest

**Table A1.** List of Data Platforms Available for Generating Objective Map of Wind Speed for NOAA HWINDS on 1 and 2 September 2004<sup>a</sup>

Data type	1 September 2004					2 September 2004				
	1:30	7:30	13:30	19:30	22:30	1:30	7:30	13:30	19:30	22:30
GPS dropwindsonde	x	x		x	x	x	x	x	x	x
Airforce Flight Winds	x	x	x			x	x	x		
Ship Anemometer	x	x		x	x	x			x	x
Drifting Buoy				x	x	x	x	x	x	x
Moored Buoy						x			x	x
Radiometer (SFMR)				x	x	x			x	x
Airport anemometers				x	x				x	x
Auto. Sfc Obs. Sys.			x	x	x	x	x		x	x
GOES satellite	x	x		x	x	x	x		x	x
QSCAT scatterometer	x	x	x			x	x	x		
SSM/I microwave sensor						x				
CMAN weather station						x				

<sup>a</sup>SFMR, stepped frequency microwave radiometer; QSCAT, quick scatterometer satellite; SSM/I, special sensor microwave/imager; GOES, geostationary operational environmental satellite; GPS, global positioning system; C-MAN, coastal marine automated network. This data was retrieved from the NOAA HWINDS website <http://www.aoml.noaa.gov/hrd/>.

sources of error in our sensitivity runs. However, this does not preclude other uncertainties from contributing significantly. In general, we cannot expect to get a closer statistical fit between simulated and measured fields, without the collection of more salinity and profile data [Black *et al.*, 2007], measurements of the surface wavefield, and wind speed and surface pressure measurements.

[45] Further progress can be expected by using a state estimation context, thereby constraining a circulation model by all available ocean data. One such effort could be to assimilate the temperature and current data into the ECCO/MIT adjoint model while treating the wind stress field as an adjustable control parameter (compare *Stammer* [2005]). Such an approach would shed more light on the detailed nature of a drag coefficient parameterization under strong wind-forcing conditions, and thus on energy dissipated through shear, than we were able to provide here.

## Appendix A: Wind Stress

[46] All simulations were forced with wind stress based on the NOAA-HWIND wind speed analysis product, which combines available storm observations into an objective map [Powell *et al.*, 1998] and is publicly available at 6-hour increments during the passage of Hurricane Frances (<http://www.aoml.noaa.gov/hrd/data-sub/wind2004.html>; see Figure 3). The accuracy of the NOAA-HWIND product therefore varies over time, as it is dependent on the available data at over a particular time window. The average position of the group of floats and drifters used in this study, over a 1-day window centered 1.5 days after the

storm passage, ranged in longitude between 66.5W and 72.5W, which corresponds to a closest approach of the storm on dates 1 and 2 September 2004. Flight level winds were available on both days in addition to other sources, as represented in Table A1. Additionally, 37 of the deployed drifters had sea surface pressure sensors, and Jan Morzel used the data from those sensors to calculate the wind speed following the gradient balance for the momentum equation (<http://www.cora.nwra.com/morzel/>). His estimate of the radial wind speed was within the standard deviation of a radial average of HWIND field on 1 September 2004 at 1:30 GMT. The surface pressure data from the drifters was not used in the HWIND analysis. The wind speed field and the position of the center of the storm were linearly interpolated using a temporal weighted average at the model timestep intervals of 240 seconds. This wind field is asymmetrical, with the strongest winds in the front right quadrant.

[47] The north and east components of wind stress were then calculated following

$$\begin{aligned}\tau_x &= \rho_a C_d S_{10} U_{10} \\ \tau_y &= \rho_b C_d S_{10} V_{10} \\ S &= (U^2 + V^2)^{0.5},\end{aligned}\quad (\text{A1})$$

where  $C_d$  is the nondimensional drag coefficient, (U, V) are the east and north components of the wind speed at 10 m height above sea level, and  $\rho_a = 1.28 \text{ kg/m}^3$  is the nominal density of air [Gill, 1982].

[48] The drag coefficient was parameterized as a function of wind speed, using four different sensitivity simulations,

**Table A2.** Wind Speed and Drag Coefficient Relationship Used for Calculation of Wind Stress<sup>a</sup>

Powell <i>et al.</i> [2003]		Black <i>et al.</i> [2007]	
Wind Speed (m/s)	$C_d (\times 10^3)$	Wind Speed (m/s)	$C_d (\times 10^3)$
0–28	<i>Large and Pond</i> [1981]	0–15	<i>Large and Pond</i> [1981]
28	2.0	15	1.46
33	2.0	20	1.7
41	1.9	22	1.8
≥50	1.5	25	1.6
		≥30	1.5

<sup>a</sup>Values are for relationships based on the measurements by Powell *et al.* [2003] (for a surface layer depth of 10–100 m) and Black *et al.* [2007]. Here  $C_d$  stands for the drag coefficient.

as shown Figure 3b. For reference, radial stress profiles on the right hand side through the storm center from those drag coefficient parameterizations are shown in Figure 3c, for the wind speed product from 1 September 2004 at 1:30 GMT. Over the range of wind speeds where observations were available, the drag coefficient relationships for *Powell* and *CBLAST* simulations were fit as piecewise linear functions to a representation of the measurement based estimates, respectively, following Table A2. For wind speeds below the observed range (15 m/s for *CBLAST* and 28 m/s for *Powell*), the drag coefficient parameterization followed the relationship by *Large and Pond* [1981], and for wind speeds above, the drag coefficient was set as a constant,  $1.5 \times 10^{-3}$  (as indicated in Table A2). For the *Donelan et al.* [2004] simulation, the drag coefficient parameterization with wind speed was modeled as a smooth hyperbolic tangent function that asymptoted to a maximum value at  $S = 30$  m/s, following their in situ and laboratory measurements. The shape function follows

$$10^{-3} \cdot [1.1 \tanh((S_{10} - 25)/5) * 0.5 - 1.1 \tanh(-25/5) * 0.5 + 1.2]. \quad (\text{A2})$$

Note that this smooth representation of the *Donelan et al.* [2004] drag coefficient curve with wind speed is constant at a value of  $1.2 \times 10^{-3}$  for speeds below 10 m/s. It does not exactly follow, but is quite similar in magnitude to the relationship by *Large and Pond* [1981] for wind speeds below 25 m/s (see Figures 3b and 3c).

[49] A symmetrical wind stress field based on NOAA-HWINDS was computed following [*Sanford et al.*, 2007] for intercomparison studies between the MIT OGCM model, which uses the KPP turbulent mixing scheme, and the PWP hurricane code and turbulent mixing scheme. This forcing field was translated at a constant speed of 5.5 m/s to the north, and is very similar to the mean radial profiles from the NOAA-HWIND product (Figure 3a).

## Appendix B: Heat Fluxes

[50] The latent heat fluxes are parameterized, following *Doney et al.* [1998], as

$$Q_{lat} = \rho_a L_v C_k U_{10} (q_a - q_s), \quad (\text{B1})$$

where the relative humidity is set to 80%, a typical value for tropical climates [*Emanuel*, 1987].

[51] The transfer coefficient,  $C_k$ , is set as a constant of  $1.3 \times 10^{-3}$  as in previous hurricane modeling studies [*Price et al.*, 1994; *Jacob et al.*, 2000; *Jacob and Shay*, 2003]. Variables  $q_a$  and  $q_s$  are the specific humidity at 10 m and just above the sea surface. The difference in specific humidity is calculated using equations presented in chapter 3.1 of *Gill* [1982]. The latent heat of vaporization ( $L_v$ ) is set as a constant  $L_v = 2.45 \times 10^6$  J/kg. In equation (B1),  $U_{10}$  is interpolated from a wind stress/wind speed curve using a *Yelland et al.* [1998] drag coefficient,

$$c_d = 10^{-3} \times (0.5 + 0.071 \times U_{10}) \quad U_{10} \geq 6 \\ c_d = 0.5 \times 10^{-3} \quad 0 \leq U_{10} \leq 6, \quad (\text{B2})$$

and the bulk formula wind stress relationship [*Doney*, 1996], as specified in equation (B3):

$$\tau_x = -\rho_a c_d U_{10}^2 \sin \theta \\ \tau_y = -\rho_a c_d U_{10}^2 \cos \theta \quad (\text{B3})$$

where  $\tau_x$  and  $\tau_y$  are the east and north components of the wind stress,  $U_{10}$  is the wind speed at 10 m,  $C_d$  is the drag coefficient as formulated by *Yelland et al.* [1998],  $\rho_a = 1.22$  kg/m<sup>3</sup> is the density of air, and  $\theta$  is the direction from which the winds come and is measured clockwise from the north.

[52] **Acknowledgments.** This work was supported by ONR (NOPP) grant N00014-99-1-1049 and NASA grant NAG5-7857. This publication is also partially based on work supported by award KUS-C1-016-04 made by King Abdullah University of Science and Technology (KAUST). Tom Sanford generously provided access to temperature profile data from three EMAPEX profiling floats. Jim Price graciously provided us with the hurricane wind-forcing field and the three-dimensional PWP code that he used in simulations of the ocean's response to Hurricane Frances. In addition, we thank the researchers and data analysts who were involved in the coupled boundary layer air-sea transfer experiment, including the members of the 53rd Weather Reconnaissance Squadron who participated in airborne deployment of the instrument array supported by the Office of Naval Research. We thank Shirley Murillo at the Atlantic Oceanographic and Meteorological Laboratory for her assistance in decoding data sources on the NOAA H\*Winds website. The advice from two anonymous reviewers greatly strengthened this paper.

## References

- Aderofo, A. (1995), *Numerical Algorithms for Use in a Dynamical Model of the Ocean*, Ph.D. thesis, pp. 1–117, Univ. of London, London, U.K.
- Black, P., E. D'Asaro, W. Drennan, J. French, P. Niiler, T. Sanford, E. Terrill, E. Walsh, and J. Zhang (2007), Air-sea exchange in hurricanes: Synthesis of observations from the coupled boundary layer air-sea transfer experiment, *Bull. Am. Meteorol. Soc.*, *88*(3), 357–374.
- Bourassa, M., D. Vincent, and W. Wood (1999), A flux parameterization including the effects of capillary waves and sea state, *J. Atmos. Sci.*, *56*, 1123–1139.
- Bye, J., and A. Jenkins (2006), Drag coefficient reduction at very high wind speeds, *J. Geophys. Res.*, *111*, C03024, doi:10.1029/2005JC003114.
- Donelan, M., B. Haus, N. Reul, W. Plant, M. Stiassnie, H. Graber, O. Brown, and E. Saltzman (2004), On the limiting aerodynamic roughness of the ocean in very strong winds, *Geophys. Res. Lett.*, *31*, L18306, doi:10.1029/2004GL019460.
- Doney, S. (1996), A synoptic atmospheric surface forcing data set and physical upper ocean model for the u.s. jgofs bermuda atlantic time series study site, *J. Geophys. Res.*, *101*, 25,615–25,634.
- Doney, S., W. Large, and F. Bryan (1998), Surface ocean fluxes and water-mass transformation rates in the coupled near climate system model, *J. Clim.*, *11*, 1420–1441.
- Emanuel, K. (1987), Towards a general theory of hurricanes, *Sci. Am.*, *76*, 371–379.
- Emanuel, K. (1995), Comments on: Global climate change and tropical cyclones: part I, *Bull. Am. Meteorol. Soc.*, *76*, 2241–2243.
- Gill, A. (1982), *Atmosphere Ocean Dynamics, Int. Geophys. Ser.*, vol. 30, Elsevier, New York.
- Grachev, A., C. Fairall, J. Hare, J. Edson, and S. Miller (2003), Wind stress vector over waves, *J. Phys. Oceanogr.*, *33*, 2408–2429.
- Greatbatch, R. (1983), On the response of the ocean to a moving storm: The nonlinear dynamics, *J. Phys. Oceanogr.*, *13*, 357–367.
- Greatbatch, R. (1984), On the response of the ocean to a moving storm: Parameters and scales, *J. Phys. Oceanogr.*, *14*(1), 59–78.
- Jacob, S., and L. Shay (2003), The role of oceanic mesoscale features on the tropical cyclone-induced mixed layer response: A case study, *J. Phys. Oceanogr.*, *33*, 649–676.
- Jacob, S., L. Shay, and A. Mariano (2000), The 3d oceanic mixed layer response to hurricane gilbert, *J. Phys. Oceanogr.*, *30*, 1407–1429.
- Jaros, E., D. Mitchell, D. Wang, and W. Teague (2007), Bottom-up determination of air-sea momentum exchange under a major tropical cyclone, *Science*, *315*, 1707–1709.
- Kudryavtsev, V. (2006), On the affect of sea drops on the atmospheric boundary layer, *J. Geophys. Res.*, *111*, C07020, doi:10.1029/2005JC002970.

- Large, W., and G. Crawford (1995), Observations and simulations of upper-ocean response to wind events during the ocean storms experiment, *J. Phys. Oceanogr.*, *25*, 2831–2852.
- Large, W., and S. Pond (1981), Open ocean flux measurements in moderate to strong winds, *J. Phys. Oceanogr.*, *11*, 324–336.
- Large, W., J. McWilliams, and S. Doney (1994), Oceanic vertical mixing: A review and a model with a non-local boundary layer parameterization, *Rev. Geophys.*, *32*, 363–403.
- Lonfat, M., F. Marks, and S. Chen (2004), Precipitation distribution in tropical cyclones using the tropical rainfall measuring mission (trmm) microwave imager: A global perspective, *Mon. Weather Rev.*, *132*, 1645–1660.
- Marshall, J., A. Adcroft, C. Hill, L. Perelman, and C. Heisey (1997a), A finite-volume, incompressible navier stokes model for studies of the ocean on parallel computers, *J. Geophys. Res.*, *102*, 5753–5766.
- Marshall, J., C. Hill, L. Perelman, and A. Adcroft (1997b), Hydrostatic, quasi-hydrostatic, and non-hydrostatic ocean modeling, *J. Geophys. Res.*, *102*, 5733–5752.
- Niwa, Y., and T. Hibiya (1997), Nonlinear processes of energy transfer from traveling hurricanes to the deep ocean internal wave field, *J. Geophys. Res.*, *102*, 12,469–12,477.
- Persson, P., J. Hare, C. Fairall, and W. Otto (2005), Air-sea interaction processes in warm and cold sectors of extratropical cyclonic storms observed during fastex, *Q. J. R. Meteorol. Soc.*, *131*, 877–912.
- Pollard, R., and R. Millard (1970), Comparisons between observed and simulated wind-generated inertial oscillations, *Deep-Sea Res.*, *17*, 813–821.
- Powell, M., S. Houston, L. Amat, and N. Morisseau-Leroy (1998), The hrd real-time hurricane wind analysis system, *J. Wind Eng. Ind. Aerod.*, *77–78*, 53–64.
- Powell, M., P. Vickery, and T. Reinhold (2003), Reduced drag coefficients for high wind speeds in tropical cyclones, *Nature*, *422*, 279–283.
- Price, J. (1981), Upper-ocean response to a hurricane, *J. Phys. Oceanogr.*, *11*, 153–175.
- Price, J. (1983), Internal wave wake of a moving storm: part I. Scales, energy budget, and observations, *J. Phys. Oceanogr.*, *13*, 949–965.
- Price, J., R. Weller, and R. Pinkel (1986), Diurnal cycling: Observations and models of the upper ocean response to diurnal heating, cooling, and wind mixing, *J. Geophys. Res.*, *91*, 8411–8427.
- Price, J., T. Sanford, and G. Forristall (1994), Forced stage response to a moving hurricane, *J. Phys. Oceanogr.*, *24*, 233–260.
- Sanford, T., J. Price, J. Girton, and D. Webb (2007), Highly resolved observations and simulations of the ocean response to a hurricane, *Geophys. Res. Lett.*, *34*(13), L13604, doi:10.1029/2007GL029679.
- Smith, S. (1980), Wind stress and heat flux over the ocean in gale force winds, *J. Phys. Oceanogr.*, *10*, 709–726.
- Stammer, D. (2005), Adjusting internal model errors through ocean state estimation, *J. Phys. Oceanogr.*, *35*, 1143–1153.
- Stammer, D., K. Ueyoshi, A. Kohl, W. Large, S. Josey, and C. Wunsch (2004), Estimating air-sea fluxes of heat, freshwater, and momentum through global ocean data assimilation, *J. Geophys. Res.*, *109*, C05023, doi:10.1029/2003JC002082.
- Wu, J. (1980), Wind-stress coefficients over sea-surface near neutral conditions - a revisit, *J. Phys. Oceanogr.*, *10*, 727–740.
- Yelland, M., B. Moat, P. Taylor, R. Pascal, J. Hutchings, and V. Cornell (1998), Wind stress measurements from the open ocean corrected for airflow distortion by the ship, *J. Phys. Oceanogr.*, *28*, 1511–1526.
- Zedler, S., T. Dickey, S. Doney, J. Price, X. Yu, and G. Mellor (2002), Analyses and simulations of the upper ocean's response to hurricane felix at the bermuda testbed mooring site: 13–23 August 1995, *J. Geophys. Res.*, *107*(C12), 3232, doi:10.1029/2001JC000969.
- Zhang, W., W. Perrie, and W. Li (2006), Impacts of waves and sea spray on midlatitude storm structure and intensity, *Mon. Weather Rev.*, *134*, 2418–2442.

J. Morzel, Rosetta Consulting, 2075 Upland Avenue, Boulder, CO 80304, USA.

P. P. Niiler, Physical Oceanography Research Division, Scripps Institution of Oceanography, 9500 Gilman Drive, La Jolla, CA 92093, USA.

D. Stammer, Institut fuer Meereskunde, Zentrum fuer Meeres- und Klimaforschung, Universitaet Hamburg, Bundesstr. 53, D-20146 Hamburg, Germany.

E. Terrill, Coastal Observing Research and Development Center, Scripps Institution of Oceanography, 9500 Gilman Drive, La Jolla, CA 92093, USA.

S. E. Zedler, Institute of Applied Mathematics and Computational Science, Texas A&M University, 513 Blocker Building, Mailstop 3143, College Station, TX 77843-3143, USA. (szedler@tamu.edu)